High-capacity room-temperature hydrogen storage of zeolitic imidazolate framework/graphene oxide promoted by platinum metal catalyst

Hu Zhou [a], Jun Zhang [b], Jian Zhang [b], Xiufen Yan [b], Xiaoping Shen [c], Aihua Yuan [b],*

[a] School of Material Science and Engineering, Jiangsu University of Science and Technology, Zhenjiang 212003, PR China
[b] School of Environmental and Chemical Engineering, Jiangsu University of Science and Technology, Zhenjiang 212003, PR China
[c] School of Chemistry and Chemical Engineering, Jiangsu University, Zhenjiang 212013, PR China

ARTICLE INFO

ABSTRACT

Pt nanoparticles (NPs) have been immobilized on the support of nanoscale zeolitic imidazolate framework (ZIF-8) and graphene oxide (GO) via a facile liquid impregnation method, in which H_2PtCl_6, $NaBH_4$ and polyvinyl alcohol (PVA) act as the Pt precursor, reducing and stabilizing agents, respectively. The resulting Pt@ZIF-8/GO composite was characterized by powder X-ray diffraction, infrared spectroscopy, scanning electron microscopy, transmission electron microscopy, X-ray photoelectron spectroscopy, inductively coupled plasma emission spectroscopy, energy dispersive spectroscopy and N_2 adsorption-desorption analysis. The results showed that Pt metal catalysts with an average size of 3.8 nm were highly dispersed and anchored tightly on the external surface of the ZIF-8/GO support. The hydrogen storage performance of Pt@ZIF-8/GO was investigated. The hydrogen storage capacity of Pt@ZIF-8/GO at 298 K and 10.0 bar is 2.2 times higher than that of the parent ZIF-8. The enhanced hydrogen storage capacity is mainly attributed to the hydrogen spillover mechanism involved in such catalytic systems. The high dispersion and small size of Pt NPs, as well as intimate contacts between the Pt dissociation source and ZIF-8/GO receptor are crucial to achieving such an obvious increase in room-temperature hydrogen storage capacity.

Introduction

Hydrogen is considered as a clean energy carrier and alternative fuel source for on-board applications. Hydrogen storage is one of the key issues for realizing the hydrogen economy [1]. Porous materials have been developed as promising candidates for hydrogen storage, among which metal-organic frameworks (MOFs) have become a rapidly

developing research area and attracted tremendous attention because of their chemically tunable structures, light weight, exceptional high surface areas and porosities [2,3]. Extraordinarily high hydrogen uptakes were achieved on porous MOFs at cryogenic temperature (e.g., 77 K) [4—6]. However, their storage capacities decrease dramatically when the temperature increases due to the weak van der Waals forces between hydrogen molecules and MOFs. In fact, high ambient-temperature hydrogen storage capacities are more desirable and important from the viewpoints of practical applications in mobile systems.

To enhance the hydrogen storage performance of adsorbents at ambient temperature, a variety of strategies have been proposed and conducted. Among them, catalytic hydrogen adsorption via spillover is an effective and promising approach [7—9]. Hydrogen spillover is typically defined as the dissociative chemisorption of hydrogen on the metals (Pt, Pd or Ni) and the subsequent migration of atomic hydrogen onto the surface of the support [10—12]. In a pioneering work by Yang group, significantly enhanced room-temperature hydrogen uptakes were achieved by physically mixing a small amount of Pt/AC (AC = active carbon) catalysts with MOFs and then building carbon bridges between them, in which the hydrogen atoms moved from Pt surface to AC support and then to MOFs. The measured hydrogen storage capacities of modified IRMOF-8 and IRMOF-1 were close to 4.0 and 3.0 wt% (100 bar, 298 K), respectively, with a factor of 8.0 compared to pure MOFs [13,14]. With this strategy, significant enhancements were also observed subsequently in the same MOF (IRMOF-1) [15] and other MOFs such as MOF-177 [16], HKUST-1 [17], MIL-101(Cr) [18,19], and $M_2(BDC)_2$dabco (M = Co, Zn; bdc = 1,4-benzenedicarboxylic acid; dabco = 1,4-diazabicyclo[2.2.2]octane) [20].

In a hydrogen spillover system, the dissociation source, the contact between the dissociation source and receptor, and the nature of receptors are considered as main factors affecting hydrogen storage capacities. Highly dispersed metal catalysts enable intimate contacts with MOFs and also with hydrogen molecules. This will undoubtedly facilitate the dissociation of hydrogen and diffusion of atomic hydrogen on the surface of MOF receptor, hence improve hydrogen storage capacities. However, many factors (such as sample amounts, mortar size, grinding time and intensity, etc.) in the physical mixing and bridge-building process could affect particle sizes and contacts between particles, and then resulted in different connectivities between particles, leading to poor reproducibility in sample preparation and storage capacities [21—26]. Recently, doping metal catalysts into MOFs is being widely studied because of the abundance of available doping techniques [27—29]. Unlike high uncertainty of the physical mixing technique, chemical doping metal catalysts onto absorbents produces identical samples and exhibits high controllability and repeatability. More importantly, the doping technique determines the size and distribution of metal NPs, and improves the contact between metal catalysts and the support. Significant enhancements of storage capacity via the direct metal doping were observed on the metal-doped adsorbents such as CNTs [30—32], ACs [33—36], MOFs [37—41] and COFs [42,43].

Recently, graphite oxide (GO) is attracting much attention in the field of gas adsorption owing to its dense array of atoms

and rich functional oxygen groups that enhance the dispersive forces and increase the porosity of materials by incorporating into composites [44,45]. For example, Bandosz and other groups have prepared several samples of MOF/GO hybrids such as MOF-5/GO [46,47], HKUST-1/GO [48], MIL-100(Fe)/GO [49], MIL-101(Cr)/GO [50], MOF-199/GO [51], MIL-53(Fe)/GO [52] and ZIF-8/GO [53]. The synergistic effects on porosity and chemistry of such composites result in a significant improvement in the adsorption of various gases (NH_3, NO_2, H_2S, H_2, CO_2) [54—61], solvents (n-hexane [62], acetone [63]) and methylene blue from wastewater [64], compared to the pristine MOFs. In fact, this enhancement can be mainly ascribed to the formation of new pores on the interface between two phases (MOF and GO) and active chemistry participating in reactive adsorption. So one may expect that MOF/GO materials can also be employed as excellent supports to incorporate metal catalysts, and then improve hydrogen storage capacities via spillover. In such metal-doped ZIF-8/GO composite system, hydrogen molecules first chemisorbed and dissociated on the surface of metal catalysts, and then hydrogen atoms migrated and diffused into the pores of MOF, as well as new pores formed at the interface between GO layers and MOF. The formation of these new pores is considerably favorable to further improve the hydrogen storage capacity. In addition, the GO component can also provide a platform for the migration, diffusion and adsorption of dissociated hydrogen atoms, which will undoubtedly facilitate the whole spillover process and then enhance the adsorption performance.

In our previous studies, Pt@GO/HKUST-1 and Pt@GO/MIL-101(Cr) composites were constructed through in situ reaction between MOF precursors and pre-prepared Pt-doped GO component [65,66]. We have demonstrated that the hydrogen storage capacities at ambient temperature for the composites could be significantly enhanced as compared to pure MOFs by exploiting hydrogen spillover. Although encouraging progress has been achieved in our case, further optimizing metal-doping methods and improving hydrogen spillover efficiency are still needed to meet the potential application of such materials in hydrogen storage. In fact, during the preparation of the Pt-doped GO precursor, the oxygen groups on the surface and edge of GO sheets would decrease upon the incorporation of Pt particles, which is not favorable for the subsequent combination of GO and MOF. To further increase the dispersion of Pt metal catalysts on the support and improve contacts between the dissociation sources and receptors, we have tried to incorporate Pt metal catalysts into the MOF/GO matrix by employing a new metal-doping method. In the process of MOF/GO preparation, the rich oxygen groups of GO can react with metal ions of MOF, which facilitated to generate the well-combined MOF/GO products. The present contribution focused on room-temperature hydrogen adsorption properties of Pt-loaded zeolitic imidazolate framework ZIF-8/GO composite (Pt@ZIF-8/GO), which was in-situ generated from the reduction of H_2PtCl_6 precursor impregnated on the ZIF-8/GO support (Scheme 1). So the formation mechanisms of the metal-doped MOF/GO composites obtained by above two methods are obviously different. Very excitingly, incorporation of Pt metal catalysts into ZIF-8/GO significantly enhanced the room-temperature hydrogen
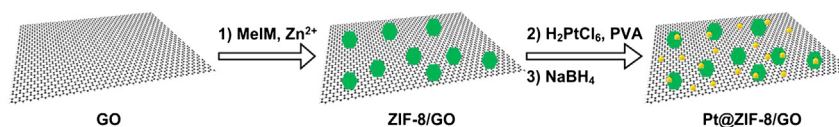
Scheme 1 – Schematic illustration of the formation process of Pt@ZIF-8/GO composite. MeIM: 2-methylimidazolate, PVA: polyvinyl alcohol. Green hexagons and yellow balls represent ZIF-8 nanocrystals and Pt NPs, respectively. (For interpretation of the references to colour in this figure legend, the reader is referred to the web version of this article.)

storage capacity by a factor of 2.2 compared to pristine ZIF-8 under the same condition. The high dispersion and small size of metal particles, and the intimate contact between Pt dissociation source and ZIF-8/GO receptor are crucial to facilitate the hydrogen spillover and thus result in an obvious enhancement in hydrogen storage capacity. To our knowledge, this is the first example of metal NPs supported on MOF/GO composites, in situ generated from chemical reduction and then doping metal catalysts into MOFs.

Experimental

Synthesis

Natural flake graphite with a particle size of 150 μm (99.9% purity) was purchased from Qingdao Guyu Graphite Co., Ltd. All chemicals and solvents are of analytical grade, purchased from Sinopharm Chemical Reagent Co., Ltd, and used without further purification.

Graphene Oxide (GO). GO was prepared by oxidation of graphite powder via a modified Hummers method [67]. In a typical synthesis, graphite powder (2.0 g) was added to concentrated H_2SO_4 (80 mL) and stirred in an ice bath. Then, $NaNO_3$ (4.0 g) and $KMnO_4$ (8.0 g) were slowly added to the suspension under stirring at temperatures below 10 °C. The reaction mixture was continually stirred for 4 h below 10 °C. Successively, the mixture was stirred at 35 °C for another 4 h, and then diluted with deionized (DI) water (200 mL). The addition of DI water was carried out in an ice bath to keep temperatures below 100 °C. The mixture was further stirred for 1 h after adding all DI water. The reaction was then terminated by adding 30% H_2O_2 solution (15 mL). The mixture was left overnight, and the solid product was separated by centrifugation, washed repeatedly with 5% HCl solution until sulfate could not be detected with $BaCl_2$. For further purification, the resulting solid was re-dispersed in DI water and then was dialyzed for 72 h to remove residual salts and acids. The suspension was dried in a vacuum oven at 60 °C for 24 h and GO was obtained.

ZIF-8. ZIF-8 was synthesized according to the similar procedure documented in the literature [68]. In a typical synthesis, a methanol solution (100 mL) of $Zn(NO_3)_2\cdot6H_2O$ (4.94 mmol, 1.467 g) was added into a methanol solution (100 mL) of 2-methylimidazole (39.52 mmol, 3.245 g) with stirring for 1 h. Stirring was stopped after combining the component solutions and a gel-like solid recovered by centrifugation. The products were washed with methanol for three times and then dried at 40 °C under vacuum.

ZIF-8/GO: A certain amount of GO (5 wt.% of the final material weight) was dispersed in methanol (30 mL) and sonicated for 5 h. The resulted GO dispersion was added into the reaction system during the preparation of ZIF-8. The resultant solution was centrifuged, washed three times with water-methanol solvent, and then dried overnight at 60 °C. Finally, the ZIF-8/GO products were activated at 160 °C under vacuum for 12 h.

Pt@ZIF-8/GO. ZIF-8/GO supported Pt metal catalysts were synthesized by in situ reduced method. Typical, 11.29 mg of polyvinyl alcohol (PVA) was introduced into the $H_2PtCl_6\cdot6H_2O$ (2.56 mL, 0.01 M) solution at room temperature. After stirring for 1 h, 100 mg of the activated ZIF-8/GO sample was added into the above solution, and the mixture was stirred for 2 h. Then, 1.28 mL of $NaBH_4$ solution (0.1 M) was added dropwise into the reaction mixture for 20 min with vigorous stirring at 0 °C. After further stirring for 5 h, the dark solids were isolated by filtration, washed two times with water (10 mL), one time with methanol followed by dry ether (10 mL). Then, the resulting product was dried overnight at 60 °C and then activated at 160 °C under vacuum for 12 h. It should be noted that though the product is named as Pt@ZIF-8/GO composite in the context, the GO component could be partially reduced during the preparation process.

ZIF-8/GO-NaBH$_4$ and ZIF-8/rGO. For comparison, the ZIF-8/GO-NaBH$_4$ and ZIF-8/rGO samples were also synthesized, and the preparation procedures are as follows. For ZIF-8/GO-NaBH$_4$, the as-synthesized ZIF-8/GO powders were treated with NaBH$_4$ under almost the same condition as the synthesis of Pt@ZIF-8/GO except for without $H_2PtCl_6\cdot6H_2O$; For ZIF-8/rGO, the GO powders were first reduced with NaBH$_4$, and then 5 wt.% of the reduced GO (rGO) was added during the preparation of ZIF-8.

Instrumentation and measurements

Powder X-ray diffraction (XRD) patterns were collected on a Shimadzu XRD-6000 diffractometer using Cu-K$_\alpha$ radiation. Fourier transform infrared spectra (FT-IR) were measured on a Nicolet FT 1703X spectrometer in the 4000–400 cm^{-1} region (KBr pellets). The morphologies and particle sizes of all samples were characterized by the scanning electron microscope (SEM, JEOL JSM-6480) and transmission electron microscopy (TEM, JEOL JEM-2100F). The elemental mapping analysis was examined by energy-dispersive X-ray spectrometry (EDS, Oxford INCA), while the Pt content was determined by

inductively coupled plasma-emission spectroscopy on an Agilent 7500ce ICP-MS. The surface electronic states were investigated by X-ray photoelectron spectroscopy (XPS, Thermo-VG Scientific ESCALAB 250 using Al Ka radiation) with a base pressure of 2×10^{-9} mbar. Low- and high-pressure gas adsorption isotherms were recorded on ASAP 2020 and 2050 volumetric instruments supplied by Micromeritics Instruments Inc, respectively. All samples were outgassed at 160 °C for 24 h prior to adsorption measurements. UHP grade N_2 and H_2 (99.999%) gases were used for all measurements. The Brunauer—Emmett—Teller (BET) specific surface areas were calculated using adsorption data in the relative pressure range from 0.06 to 0.30. The total pore volumes were calculated by a single point method at $P/P_0 = 0.99$. The pore size distribution curves were determined from the analysis of the adsorption branch of the isotherm using the Horvath—Kawazoe method.

Results and discussion

Powder X-ray diffraction

Powder X-ray diffraction patterns of all materials are shown in Fig. 1. The strong peak at $2\theta = 9.12°$ for GO sample corresponds to the (0 0 1) crystal plane, indicating an interlayer spacing of about 9.70 Å determined by Bragg's law. The characteristic diffraction peaks of as-prepared ZIF-8 match well with those derived from single-crystal X-ray diffraction data [69,70], confirming the successful preparation of the MOF of ZIF-8. The ZIF-8/GO support shows almost identical pattern to the parent ZIF-8 and no apparent loss of crystallinity, demonstrating that the incorporation of GO did not disturb or destroy the assembly of Zn(II) centers and 2-methylimidazole ligands to
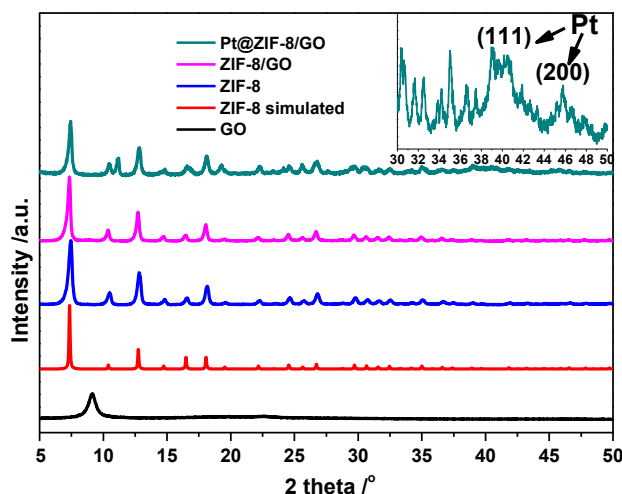
form ZIF-8. The characteristic peaks of GO were not detected in the pattern of ZIF-8/GO, which can be ascribed to the low content of GO or/and the exfoliation/high dispersion of GO in the composite [71]. The Pt@ZIF-8/GO composite also adopts similar diffraction pattern to the ZIF-8/GO and ZIF-8 products, suggesting that the framework of ZIF-8/GO was well preserved despite of the loading of Pt metal catalyst. However, the diffraction intensities of Pt@ZIF-8/GO decrease slightly with respect to the ZIF-8/GO support, which could be due to the loss in the crystallinity and/or structural distortion caused by the incorporation of Pt particles into the ZIF-8/GO network. The characteristic diffraction peaks ascribed to Pt(0) species at around 40° and 46° were detected from the diffraction pattern of Pt@ZIF-8/GO, demonstrating the presence of Pt particles in the composite. The broad peaks and weak intensities can be reasonably attributed to the very small size and high dispersion of Pt particles in the composite as shown in TEM images.

FT-IR spectra

FT-IR spectra of all materials are shown in Fig. 2. The characteristic peaks of GO are well consistent with the fingerprint groups [72,73]. The broad band at 3698—3000 cm^{-1} can be attributed to the hydroxyl stretching vibration of water and C—OH group of GO. The band at 1720 cm^{-1} corresponds to stretching vibrations of the C=O bonds of carbonyl and/or carboxyl groups. The bands at 1630 and 1385 cm^{-1} are assigned to vibrations of the O—H bonds in water and C—OH groups, respectively. The C—O bonds are observed as the intense band appeared at 1054 cm^{-1}. The adsorption bands for ZIF-8 at 3135 and 2928 cm^{-1} are associated with the aromatic and the aliphatic C—H stretch of the imidazole. The C=N stretch appeared at 1584 cm^{-1}, while the intense and convoluted bands at 1500—1350 cm^{-1} are assigned to the entire ring stretching. The wavenumber region of 1350—900 cm^{-1} exhibits various bands assigned to the in-plane bending of the ring, whereas those below 800 cm^{-1} are ascribed to the out-of-plane bending. The IR spectrum of as-prepared ZIF-8 is agreement with the reported data [53,74,75]. It should be noted

Fig. 1 — Powder XRD patterns of GO, ZIF-8, ZIF-8/GO and Pt@ZIF-8/GO (Red line represents XRD pattern simulated from single-crystal structural data of ZIF-8). Inset: XRD pattern at $2\theta = 30$-$50°$ for Pt@ZIF-8/GO measured with the slow scanning speed of 1°/min. (For interpretation of the references to colour in this figure legend, the reader is referred to the web version of this article.)
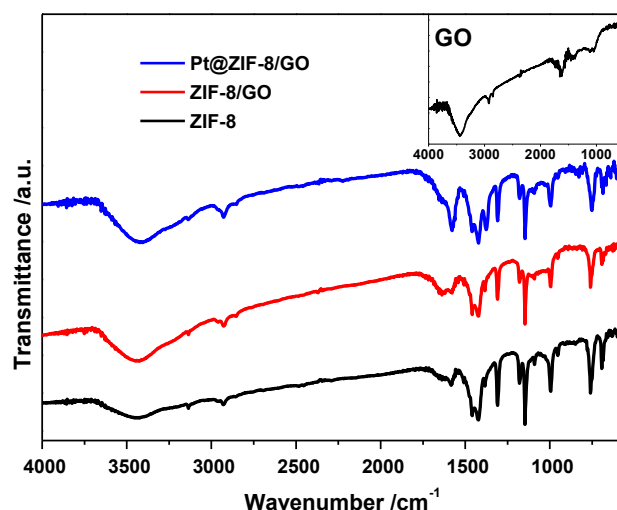
Fig. 2 — FT-IR spectra of GO (inset), ZIF-8, ZIF-8/GO and Pt@ZIF-8/GO.

that the vibration bands related to functional groups of GO are not seen in ZIF-8/GO and Pt@ZIF-8/GO samples, probably due to the much lower content of GO component. In addition, both ZIF-8/GO and Pt@ZIF-8/GO exhibit identical bands to the pristine ZIF-8, indicating the incorporation of GO and Pt metal catalyst did not prevent the coordination of 2-methylimidazole linker to the zinc(II) centers, and thus the formation of ZIF-8 component. Above analysis supports the results drawn from the powder XRD experiments.

Morphologies

Pt@ZIF-8/GO and ZIF-8/GO samples show much darker color than the parent ZIF-8 (Fig. 3a), indicating the good incorporation of GO and Pt components into the ZIF-8 matrix. The morphology of the parent material and the composites was investigated by SEM and TEM. As shown in Fig. 3b, GO exhibits curled and corrugated layered structure. The ZIF-8 crystals have nanoscale size and show obvious aggregation (Fig. 3c), while ZIF-8 nanocrystals in ZIG-8/GO and Pt@ZIF-8/GO samples are randomly dispersed on GO sheets (Fig. 3d, e). Furthermore, ZIF-8 nanocrystals in both the composites exhibit similar morphology and particle size to the pristine ZIF-8. Although Pt NPs in Pt@ZIF-8/GO cannot be observed in the SEM image due to their small size, the EDS analysis

indicates that the C, O, Zn and Pt elements are uniformly dispersed in Pt@ZIF-8/GO, suggesting that Pt NPs are loaded throughout the whole ZIF-8/GO network (Fig. S1). The ICP-MS measurement shows that the Pt@ZIF-8/GO composite has a Pt loading of 1.82 wt.%.

The XPS study was carried out to elucidate the oxidation state of Pt species and the surface composition of Pt@ZIF-8/GO, as shown in Fig. 4. The survey scan XPS spectrum indicates the presence of Pt in addition to the elements (Zn, C, N, O) of ZIF-8/GO. Two prominent peaks with binding energies of 71.1 and 74.5 eV can be readily assigned to the signals of Pt(0) $4f_{7/2}$ and Pt(0) $4f_{5/2}$ levels, respectively, demonstrating the efficient reduction of Pt(IV) to Pt(0) after in situ treatments with $NaBH_4$ during the composite preparation. The binding energy difference of 3.4 eV for above two peaks is in good accordance with the theoretical value [76].

The typical TEM images of all the samples are shown in Fig. 5 and Fig. S2. GO is seen as dense flakes of graphene layers stacked together by dispersive forces (Fig. 5a), while ZIF-8 exhibits well-defined and uniform hexagonal morphology with the average diameter of 56 nm (Fig. 5b, Fig. S2a). Similar hexagonal morphology and particle size of ZIF-8 are also found in the ZIF-8/GO support (Fig. 5c, Fig. S2b), where ZIF-8 crystals are homogeneously distributed on a few irregular GO sheets. Notably, ZIF-8 crystals in the Pt@ZIF/GO composite
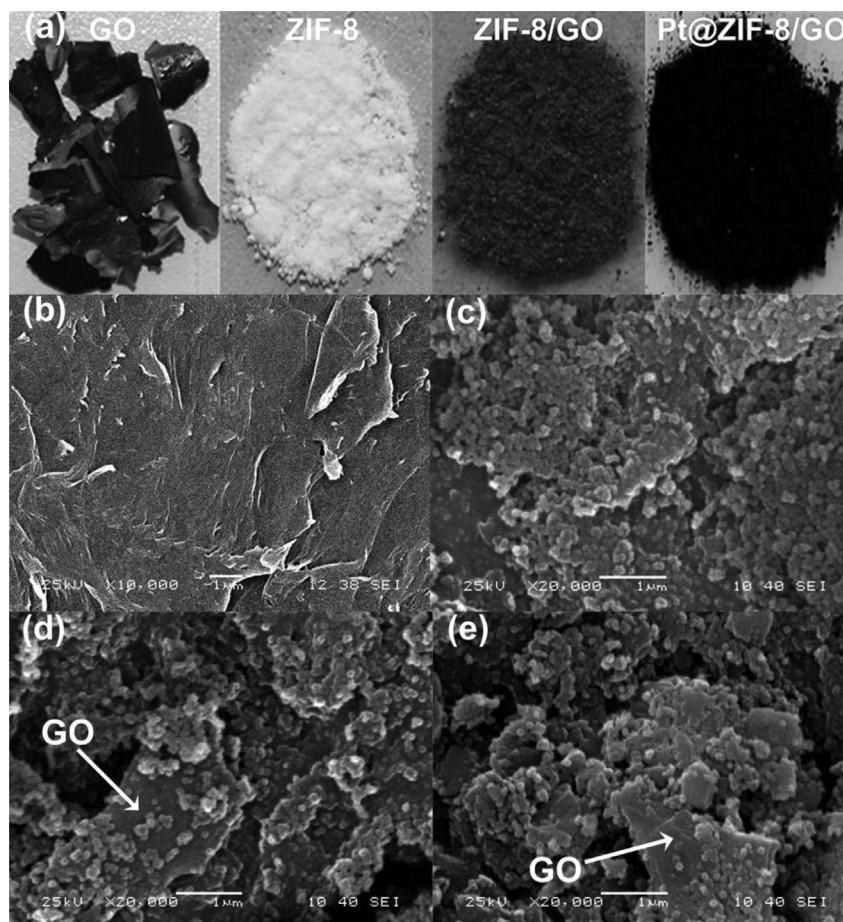

Fig. 3 — (a) Digital photographs of the as-synthesized samples, and SEM images of (b) GO, (c) ZIF-8, (d) ZIF-8/GO and (e) Pt@ZIF-8/GO.
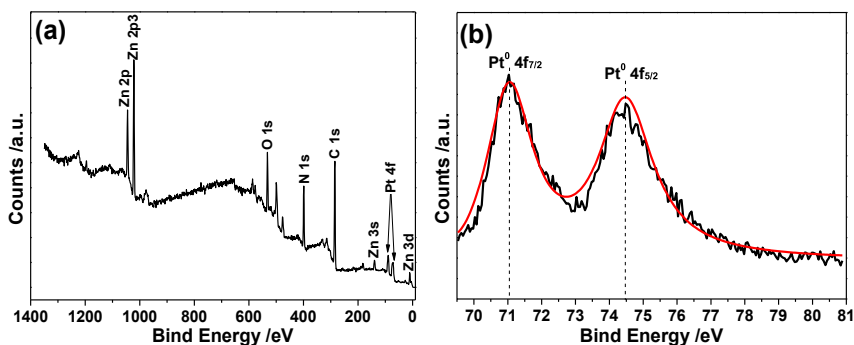
Fig. 4 – (a) Survey scan XPS spectrum of Pt@ZIF-8/GO, (b) high resolution Pt 4f XPS spectrum (black line) for Pt@ZIF-8/GO and its simulated peak (red line). (For interpretation of the references to colour in this figure legend, the reader is referred to the web version of this article.)
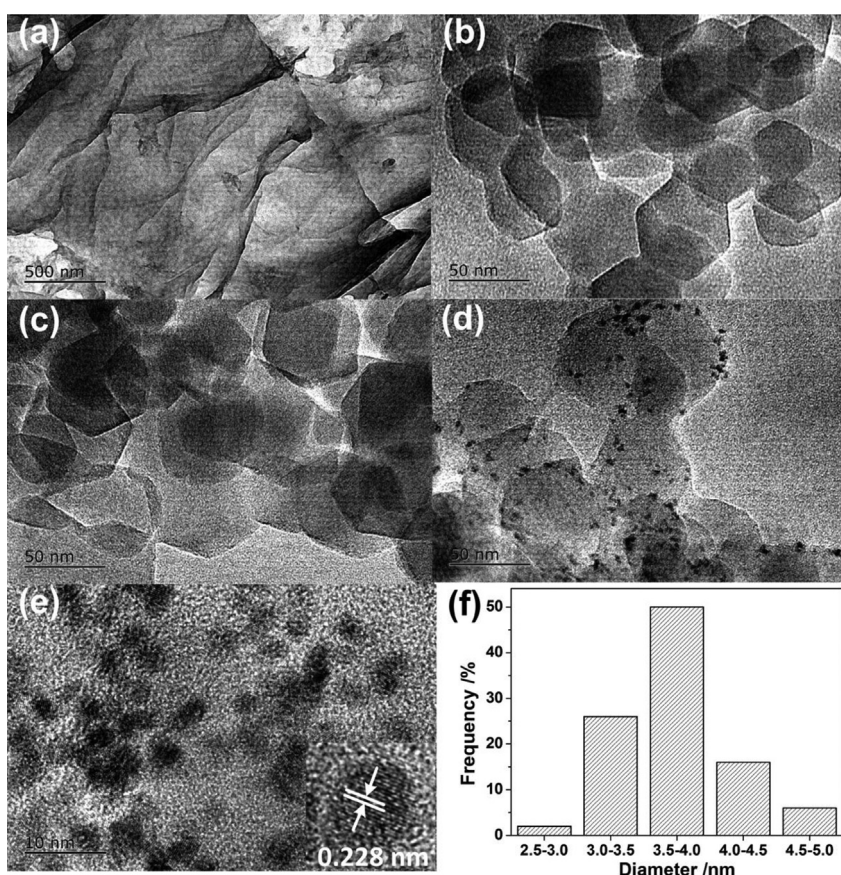

Fig. 5 – TEM images of (a) GO, (b) ZIF-8, (c) ZIF-8/GO and (d, e) Pt@ZIF-8/GO. The inset of (e) is high-resolution TEM image of a Pt NP. (f) The corresponding size distribution plot of Pt NPs.

show no significant change or collapse in morphology and structure as compared with the matrix ZIF-8 and ZIF-8/GO support (Fig. 5d, Fig. S2c, Fig. S2d). Furthermore, Pt NPs are effectively immobilized onto the ZIF-8/GO network. The high magnification TEM image (Fig. 5e) reveals that Pt NPs exist as black dots with an average size of approximately 3.8 nm calculated from a statistical evaluation of 70 particles. The inset of Fig. 5e shows the high-resolution TEM image of a Pt NPs, from which clear lattice fringes with a spacing of 0.228 nm can be observed, which correspond to Pt(111) planes [77]. This indicates that Pt metal catalysts are randomly located on external surface and edges of ZIF-8 since they are much bigger than the pores in the structure of ZIF-8, which contains large cavities (1.16 nm of diameter) interconnected by narrow windows (0.34 nm of diameter) [67]. No significant aggregation of Pt NPs observed in our composite can be mainly
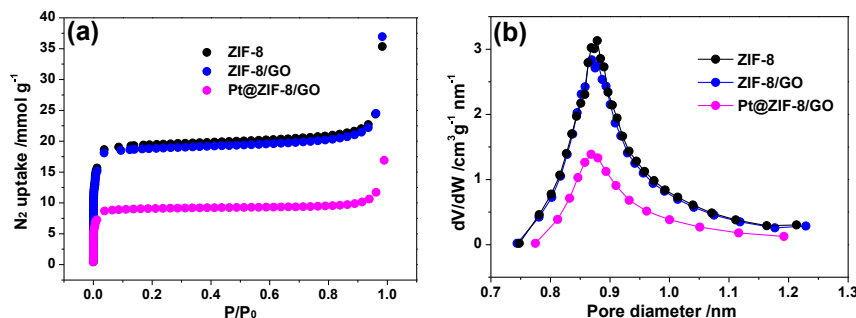
Fig. 6 – (a) Nitrogen adsorption isotherms at 77 K and (b) the pore size distribution curves calculated by the Horvath–Kawazoe method for ZIF-8, ZIF-8/GO, and Pt@ZIF-8/GO samples.

attributed to the fact that PVA acted as a protecting agent in the course of preparation. In addition, the presence of GO may be also a contributing factor because GO sheets can provide platforms for the dispersion of Pt NPs, despite of a quite small content in the composite.

Textures

The specific surface areas of all samples were determined by nitrogen physisorption, as shown in Fig. 6a, and the textural parameters are given in Table 1. GO exhibits nonporous feature (not shown here), while ZIF-8, ZIF-8/GO and Pt@ZIF-8/GO show typical type-I isotherms, characteristic of microporous materials [78]. The measured BET surface area of ZIF-8 is 1297 $m^2 g^{-1}$, close to the reported values [79–81]. The surface area of 1247 $m^2 g^{-1}$ for ZIF-8/GO is slightly reduced relative to ZIF-8, arising from the introduction of nonporous GO component. It is noteworthy that the BET value (1247 $m^2 g^{-1}$) measured for ZIF-8/GO is slightly higher than the hypothetical one (1232 $m^2 g^{-1}$), which was calculated based on the physical mixture of the components of GO and ZIF-8 as well as the content of each component in the composite. This result can be reasonably ascribed to the synergistic effect between GO and ZIF-8 components, where new pores were formed at the interface between GO layers and ZIF-8, as observed in other MOF/GO (MOF = MOF-5, HKUST-1, MIL-100(Fe)) materials [46,48,49]. The formation of new pores can be further confirmed by the increase of pore volumes from 1.225 $cm^3 g^{-1}$ of ZIF-8 to 1.281 $cm^3 g^{-1}$ of ZIF-8/GO. Compared with the pure ZIF-8 and ZIF-8/GO support, the BET surface area (637 $m^2 g^{-1}$) and pore volume (0.586 $cm^3 g^{-1}$) of the Pt@ZIF-8/GO composite obviously decreased. Considering the fact that Pt NPs have a much larger particle size of 3.8 nm determined by TEM image than the cavity of ZIF-8, Pt NPs are not located in the
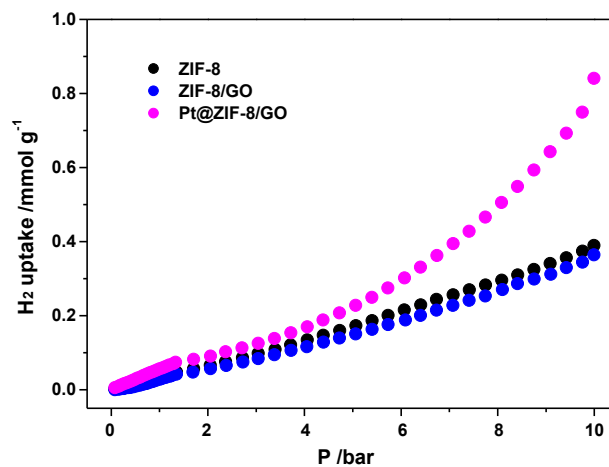

Fig. 7 – High-pressure hydrogen adsorption isotherms at 298 K for ZIF-8, ZIF-8/GO and Pt@ZIF-8/GO.

supercages of ZIF-8 but encapsulated in the ZIF-8/GO network instead. So the expected loss of BET surface area for Pt@ZIF-8/GO can be ascribed to the fact that the cages of ZIF-8 are blocked by Pt NPs and/or the residual PVA (acting as a protecting agent in the preparation process), which could be deposited at the pore surface. A narrow pore size distribution of ZIF-8 calculated by the Horvath–Kawazoe method displays the pore size centered at 0.87 nm (Fig. 6b). In comparison with the host ZIF-8, the incorporation of GO and Pt NPs does not alter the pore size distribution of the MOF matrix, although the appreciable decrease was observed (especially for Pt@ZIF-8/GO). This is consistent with the fact that the introduced Pt

Table 1 – Surface areas, pore volumes, and hydrogen uptakes at 298 K for the as-synthesized samples.				
Sample	S_{BET} ($m^2 g^{-1}$)	V_{total} ($cm^3 g^{-1}$)	H_2 uptake (298 K, 1.13 bar) (mmol g^{-1})	H_2 uptake (298 K, 10.0 bar) (mmol g^{-1})
ZIF-8	1297	1.225	0.036	0.390
ZIF-8/GO	1247	1.281	0.028	0.364
Pt@ZIF-8/GO	619	0.586	0.402	0.841

catalyst particles are too large to occupy the pore space, but locate at the exterior surface of ZIF-8 units.

Hydrogen adsorption capacity

The high-pressure hydrogen adsorption isotherms at 298 K for ZIF-8, ZIF-8/GO and Pt@ZIF-8/GO materials are shown in Fig. 7. ZIF-8 has a hydrogen uptake of 0.390 mmol g^{-1} at 10.0 bar, close to the reported value under the similar condition [82]. The introduction of nonporous GO component caused a slight loss in the adsorption capacity for ZIF-8/GO (0.364 mmol g^{-1}, 10.0 bar). It is noteworthy that the hydrogen storage capacity (0.841 mmol g^{-1}, 10.0 bar) of the Pt@ZIF-8/GO composite has significantly enhanced with a factor of 2.2 compared to ZIF-8 after doping a small amount of Pt metal catalyst into the ZIF-8/GO support. Apparently, more hydrogen gas would be adsorbed with further increasing the pressure from the isotherm. It is obvious that the improved hydrogen storage capacity at 298 K cannot be attributed to the difference in specific surface area because of the obviously decreased BET value for Pt@ZIF-8/GO compared to ZIF-8. The enhancement in hydrogen storage capacity can be mainly ascribed to the spillover of atomic hydrogen from Pt metal catalyst to ZIF-8/GO receptor. It was reported that the increased hydrogen storage capacities can be achieved on absorbents including carbon materials [83—90], polystyrene [91], organic polymers [92], and MOFs by doping metal catalysts to induce hydrogen spillover at ambient temperatures [8,9,93—95]. In general, the metal NPs and MOFs in these materials act as the spillover source of hydrogen molecules and receptors, respectively. Similarly, Pt NPs in our composite act as the hydrogen spillover source, and intimate contact between Pt particles and ZIF-8/GO receptor leads to a lower energy barrier for the spillover of dissociated hydrogen from Pt particles to the receptor. Thus, hydrogen molecules first chemisorbed and dissociated on the surface of Pt metal catalyst, and then migrated and further diffuse into the surface and internal pores of the receptor ZIF-8/GO (Scheme 2). The present research indicated that high dispersion and small sizes of metal catalysts could facilitate spillover process on adsorbents and in turn favor an obvious increase in the storage capacity at 298 K. The 2.2-fold enhancement for the Pt@ZIF-8/GO composite indicated that the spillover effect has a considerable influence on the final hydrogen adsorption
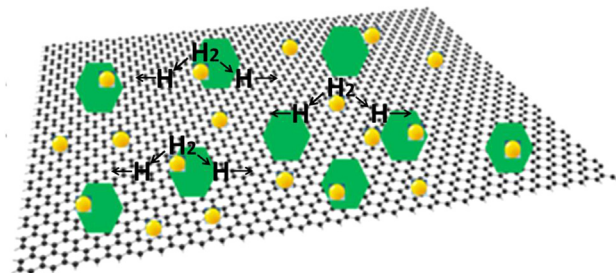
amount of the metal-doped absorbents. Similarly, a significant enhancement with a factor of 11.2 in hydrogen storage capacity at 298 K and 1.13 bar was observed for Pt@ZIF-8/GO with respect to ZIF-8 from low-pressure adsorption isotherms (Fig. S3). In addition, the ZIF-8/GO sample treated with NaBH$_4$ (ZIF-8/GO-NaBH$_4$), and ZIF-8/rGO have also been prepared and compared to the Pt@ZIF-8/GO composite. Powder XRD patterns (Fig. S4) of both the samples exhibit identical features to the pristine ZIF-8 and the untreated ZIF-8/GO, indicating the framework of ZIF-8 was well retained in these two materials. In fact, the hydrogen uptake amounts (Fig. S5) of both the materials are much lower than that of the Pt@ZIF-8/GO composite, further confirming the presence of spillover effect in Pt@ZIF-8/GO system. The hydrogen adsorption experiment at 298 K for the second time of the Pt@ZIF-8/GO composite indicates a high reproducibility of the result (Fig. S5).

Conclusions

In summary, we have demonstrated that the Pt@ZIF-8/GO composite could be obtained by chemical impregnation of the ZIF-8/GO support with the H$_2$PtCl$_6$ solution followed by a reduction treatment, in which Pt NPs were highly dispersed and anchored tightly on the external surface of ZIF-8/GO support. The significantly enhanced room-temperature hydrogen uptake of Pt@ZIF-8/GO compared to the pristine ZIF-8 is mainly ascribed to the catalytic spillover mechanism. The high dispersion and uniform small size of Pt metal catalyst, as well as intimate contacts between metal dissociation source and ZIF-8/GO receptor are crucial to facilitate the spillover process. The current work may open an opportunity for the development of potentially suitable candidate materials for hydrogen storage at ambient conditions by using MOF/GO as an effective support to immobilize metallic catalysts. Furthermore, metal-assisted storage via catalytic spillover has been shown as one of the most promising approaches for hydrogen storage at ambient temperature. Further work is underway in our laboratory to improve and optimize the composite preparation and investigate the factors affecting the spillover mechanism involved in such catalytic systems.

Scheme 2 — The hydrogen spillover mechanism in the Pt@ZIF-8/GO composite. Green hexagons and yellow balls represent ZIF-8 nanocrystals and Pt NPs, respectively. (For interpretation of the references to colour in this figure legend, the reader is referred to the web version of this article.)

Appendix A. Supplementary data

Supplementary data related to this article can be found at http://dx.doi.org/10.1016/j.ijhydene.2015.05.199.

REFERENCES

[1] Schlapbach L, Züttel A. Hydrogen-storage materials for mobile applications. Nature 2001;414:353–8.

[2] Furukawa H, Cordova KE, O'Keeffe M, Yaghi OM. The chemistry and applications of metal-organic frameworks. Science 2013;341:1230444.

[3] Zhou HC, Long JR, Yaghi OM. Introduction to metal-organic frameworks. Chem Rev 2012;112:673–4.

[4] Suh MP, Park HJ, Prasad TK, Lim DW. Hydrogen storage in metal-organic frameworks. Chem Rev 2012;112:782–835.

[5] Sculley J, Yuan DQ, Zhou HC. The current status of hydrogen storage in metal-organic frameworks-updated. Energy Environ Sci 2011;4:2721–35.

[6] Ren JW, Langmi HW, North BC, Mathe M. Review on processing of metal-organic framework (MOF) materials towards system integration for hydrogen storage. Int J Energy Res 2015;39:607–20.

[7] Wang LF, Yang RT. Hydrogen storage on carbon-based adsorbents and storage at ambient temperature by hydrogen spillover. Catal Rev 2010;52:411–61.

[8] Wang LF, Yang RT. New sorbents for hydrogen storage by hydrogen spillover – a review. Energy Environ Sci 2008;1:268–79.

[9] Wang LF, Lachawiec Jr AJ, Yang RT. Nanostructured adsorbents for hydrogen storage at ambient temperature: high-pressure measurements and factors influencing hydrogen spillover. RSC Adv 2013;3:23935–52.

[10] Robell AJ, Ballou EV, Boudart M. Surface diffusion of hydrogen on carbon. J Phys Chem 1964;68:2748–53.

[11] Srinivas ST, Rao PK. Direct observation of hydrogen spillover on carbon-supported platinum and its influence on the hydrogenation of benzene. J Catal 1994;148:470–7.

[12] Conner Jr WC, Falconer JL. Spillover in heterogeneous catalysis. Chem Rev 1995;95:759–88.

[13] Li YW, Yang RT. Significantly enhanced hydrogen storage in metal-organic frameworks via spillover. J Am Chem Soc 2006;128:726–7.

[14] Li YW, Yang RT. Hydrogen storage in metal-organic frameworks by bridged hydrogen spillover. J Am Chem Soc 2006;128:8136–7.

[15] Lee SY, Park SJ. Effect of platinum doping of active carbon on hydrogen storage behaviors of metal-organic frameworks-5. Int J Hydrogen Energy 2011;36:8381–7.

[16] Li YW, Yang RT. Gas adsorption and storage in metal-organic framework MOF-177. Langmuir 2007;23:12937–44.

[17] Li YW, Yang RT. Hydrogen storage in metal-organic and covalent-organic frameworks by spillover. AIChE J 2008;54:269–79.

[18] Liu YY, Zeng JL, Zhang J, Xu F, Sun LX. Improved hydrogen storage in the modified metal-organic frameworks by hydrogen spillover effect. Int J Hydrogen Energy 2007;32:4005–10.

[19] Klyamkin SN, Chuvikov SV, Maletskaya NV, Kogan EV, Fedin VP, Kovalenko KA, et al. High-pressure hydrogen storage on modified MIL-101 metal-organic framework. Int J Energy Res 2014;38:1562–70.

[20] Lin KS, Adhikari AK, Chang KC, Chiang CL, Wang CH. Synthesis, characterization, and hydrogen storage enhancement of $M_2(BDC)_2$dabco with palladium-doped activated carbon. J Nanosci Nanotechnol 2014;14:2700–8.

[21] Luzan SM, Talyzin AV. Hydrogen adsorption in Pt catalyst/MOF-5 materials. Microporous Mesoporous Mater 2010;135:201–5.

[22] Li YW, Yang FH, Yang RT. Response to "hydrogen adsorption in Pt catalyst/MOF-5 materials" by Luzan and Talyzin. Microporous Mesoporous Mater 2010;135:206–8.

[23] Hirscher M. Remarks about spillover and hydrogen adsorption – comments on the contributions of AV Talyzin and RT Yang. Microporous Mesoporous Mater 2010;135:209–10.

[24] Luzan SM, Talyzin AV. Comment to the "response to hydrogen adsorption in Pt catalyst/MOF-5 materials" by Li et al. Microporous Mesoporous Mater 2010;139:216–8.

[25] Campesi R, Cuevas F, Latroche M, Hirscher M. Hydrogen spillover measurements of unbridged and bridged metal-organic frameworks-revisited. Phys Chem Chem Phys 2010;12:10457–9.

[26] Stuckert NR, Wang LF, Yang RT. Characteristics of hydrogen storage by spillover on Pt-doped carbon and catalyst-bridged metal organic framework. Langmuir 2010;26:11963–71.

[27] Moon HR, Lim DW, Suh MP. Fabrication of metal nanoparticles in metal-organic frameworks. Chem Soc Rev 2013;42:1807–24.

[28] Meilikhov M, Yusenko K, Esken D, Turner S, Tendeloo GV, Fischer RA. Metals@MOFs – loading MOFs with metal nanoparticles for hybrid functions. Eur J Inorg Chem 2010:3701–14.

[29] Dhakshinamoorthy A, Carcia H. Catalysis by metal nanoparticles embedded on metal-organic frameworks. Chem Soc Rev 2012;41:5262–84.

[30] Singh P, Kulkarni MV, Gokhale SP, Chikkali SH, Kulkarni CV. Enhancing the hydrogen storage capacity of Pd-functionalized multi-walled carbon nanotubes. Appl Surf Sci 2012;258:3405–9.

[31] Chen CY, Chang JK, Tsai WT. Improved hydrogen storage performance of defected carbon nanotubes with Pd spillover catalysts dispersed using supercritical CO_2 fluid. Int J Hydrogen Energy 2012;37:3305–12.

[32] Tsai PJ, Yang CH, Hsu EC, Tsai WT, Chang JK. Enhancing hydrogen storage on carbon nanotubes via hybrid chemical etching and Pt decoration employing supercritical carbon dioxide fluid. Int J Hydrogen Energy 2012;37:6714–20.

[33] Figueroa-Torres MZ, Domínguez-Ríos C, Cabañas-Moreno JG, Vega-Becerra O, Aguilar-Elguézabal A. The synthesis of Ni-activated carbon nanocomposites via electroless deposition without a surface pretreatment as potential hydrogen storage materials. Int J Hydrogen Energy 2012;37:10743–9.

[34] Wang Y, Wang K, Guan C, He ZM, Lu ZS, Chen T, et al. Surface functionalization-enhanced spillover effect on hydrogen storage of Ni–B nanoalloy-doped activated carbon. Int J Hydrogen Energy 2011;36:13663–8.

[35] Li QX, Lueking AD. Effect of surface oxygen groups and water on hydrogen spillover in Pt-doped activated carbon. J Phys Chem C 2011;115:4273–82.

[36] Chen H, Yang RT. Catalytic effects of TiF_3 on hydrogen spillover on Pt/carbon for hydrogen storage. Langmuir 2010;26:15394–8.

[37] Szilágyi PÁ, Callini E, Anastasopol A, Kwakernaak C, Sachdeva S, van de Krol R, et al. Probing hydrogen spillover in Pd@MIL-101(Cr) with a focus on hydrogen chemisorptions. Phys Chem Chem Phys 2014;16:5803–9.

[38] Chen H, Wang LF, Yang J, Yang RT. Investigation on hydrogenation of metal-organic frameworks HKUST-1, MIL-53, and ZIF-8 by hydrogen spillover. J Phys Chem 2013;C117:7565–76.

[39] Wang L, Stuckert NR, Chen H, Yang RT. Effects of Pt particle size on hydrogen storage on Pt-doped metal-organic framework IRMOF-8. J Phys Chem C 2011;115:4793–9.

[40] Zlotea C, Campesi R, Cuevas F, Leroy E, Dibandjo P, Volkringer C, et al. Pd nanoparticles embedded into a metal-organic framework: synthesis, structural characteristics, and hydrogen sorption properties. J Am Chem Soc 2010;132:2991–7.

[41] Proch S, Herrmannsdofer J, Kempe R, Kern C, Jess A, Seyfarth L, et al. Pt@MOF-177: synthesis, room-temperature hydrogen storage and oxidation catalysis. Chem Eur J 2008;14:8204−12.

[42] Kalidindi SB, Fischer RA. Covalent organic frameworks and their metal nanoparticle composites: prospects for hydrogen storage. Phys Status Solidi B 2013;250:1119−27.

[43] Kalidindi SB, Oh H, Hirscher M, Esken D, Wiktor C, Turner S, et al. Metal@COFs: covalent organic frameworks as templates for Pd nanoparticles and hydrogen storage properties of hybrid material. Chem Eur J 2012;18:10848−56.

[44] Dreyer DR, Park S, Bielawski CW, Ruoff RS. The chemistry of graphene oxide. Chem Soc Rev 2010;39:228−40.

[45] Huang X, Qi X, Boey F, Zhang H. Graphene-based composites. Chem Soc Rev 2012;41:666−86.

[46] Petit C, Bandosz TJ. MOF-graphite oxide composites: combining the uniqueness of graphene layers and metal-organic frameworks. Adv Mater 2009;21:4753−7.

[47] Jahan M, Bao QL, Yang JX, Loh KP. Structure-directing role of graphene in the synthesis of metal-organic framework nanowire. J Am Chem Soc 2010;132:14487−95.

[48] Petit C, Burress J, Bandosz TJ. The synthesis and characterization of copper-based metal-organic framework/graphite oxide composites. Carbon 2011;49:563−72.

[49] Petit C, Bandosz TJ. Synthesis, characterization, and ammonia adsorption properties of mesoporous metal-organic framework (MIL(Fe))-graphite oxide composites: exploring the limits of materials fabrication. Adv Funct Mater 2011;21:2108−17.

[50] Ahmed I, Khan NA, Jhung SH. Graphite oxide/metal-organic framework (MIL-101): remarkable performance in the adsorptive denitrogenation of model fuels. Inorg Chem 2013;52:14155−61.

[51] Zhang SL, Du Z, Li GK. Metal-organic framework-199/graphite oxide hybrid composites coated solid-phase microextraction fibers coupled with gas chromatography for determination of organochlorine pesticides from complicated samples. Talanta 2013;115:32−9.

[52] Zhang Y, Li G, Lu H, Lv Q, Sun ZG. Synthesis, characterization and photocatalytic properties of MIL-53(Fe)-graphene hybrid materials. RSC Adv 2014;4:7594−600.

[53] Kumar R, Jayaramulu K, Maji TK, Rao CNR. Hybrid nanocomposites of ZIF-8 with graphene oxide exhibiting tunable morphology, significant CO_2 uptake and other novel properties. Chem Commun 2013;49:4947−9.

[54] Petit C, Mendoza B, Bandosz TJ. Reactive adsorption of ammonia on Cu-based MOF/graphene composites. Langmuir 2010;26:15302−9.

[55] Petit C, Bandosz TJ. Enhanced adsorption of ammonia on metal-organic framework/graphite oxide composites: analysis of surface interactions. Adv Funct Mater 2010;20:111−8.

[56] Levasseur B, Petit C, Bandosz TJ. Reactive adsorption of NO_2 on copper-based metal-organic framework and graphite oxide/metal-organic framework composites. ACS Appl Mater Inter 2010;2:3606−13.

[57] Petit C, Mendoza B, Bandosz TJ. Hydrogen sulfide adsorption on MOFs and MOF/graphite oxide composites. Chemphyschem 2010;11:3678−84.

[58] Petit C, Bandosz TJ. Exploring the coordination chemistry of MOF-graphite oxide composites and their applications as adsorbents. Dalton Trans 2012;41:4027−35.

[59] Petit C, Levasseur B, Mendoza B, Bandosz TJ. Reactive adsorption of acidic gases on MOF/graphite oxide composites. Microporous Mesoporous Mater 2012;154:107−12.

[60] Petit C, Wrabetz S, Bandosz TJ. Microcalorimetric insight into the analysis of the reactive adsorption of ammonia on Cu-

MOF and its composite with graphite oxide. J Mater Chem 2012;22:21443−7.

[61] Liu S, Sun LX, Xu F, Zhang J, Jiao CL, Li F, et al. Nanosized Cu-MOFs induced by graphene oxide and enhanced gas storage capacity. Energy Environ Sci 2013;6:818−23.

[62] Sun XJ, Xia QB, Zhao ZX, Li YW, Li Z. Synthesis and adsorption performance of MIL-101(Cr)/graphite oxide composites with high capacities of n-hexane. Chem Eng J 2014;239:226−32.

[63] Zhou X, Huang WY, Shi J, Zhao ZX, Xia QB, Li YW, et al. A novel MOF/graphene oxide composite GrO@MIL-101 with high adsorption capacity for acetone. J Mater Chem A 2014;2:4722−30.

[64] Li L, Liu XL, Geng HY, Hu B, Song GW, Xu ZS. A MOF/graphite oxide hybrid (MOF: HKUST-1) material for the adsorption of methylene blue from aqueous solution. J Mater Chem A 2013;1:10292−9.

[65] Zhou H, Liu XQ, Zhang J, Yan XF, Liu YJ, Yuan AH. Enhanced room-temperature hydrogen storage capacity in Pt-loaded graphene oxide/HKUST-1 composites. Int J Hydrogen Energy 2014;39:2160−7.

[66] Zhang J, Liu XQ, Zhou H, Yan XF, Liu YJ, Yuan AH. Pt-doped graphene oxide/MIL-101 nanocomposites exhibiting enhanced hydrogen uptake at ambient temperature. RSC Adv 2014;4:28908−13.

[67] Hummers WS, Offeman RE. Preparation of graphitic oxide. J Am Chem Soc 1958;80:1339.

[68] Cravillon J, Münzer S, Lohmeier SJ, Feldhoff A, Huber K, Wiebcke M. Rapid room-temperature synthesis and characterization of nanocrystals of a prototypical zeolitic imidazolate framework. Chem Mater 2009;21:1410−2.

[69] Park KS, Ni Z, Côté AP, Choi JY, Huang R, Uribe-Romo FJ, et al. Exceptional chemical and thermal stability of zeolitic imidazolate frameworks. Proc Natl Acad Sci U S A 2006;103:10186−91.

[70] Huang XC, Lin YY, Zhang JP, Chen XM. Ligand-directed strategy for zeolite-type metal-organic frameworks: zinc(II) imidazolates with unusual zeolitic topologies. Angew Chem Int Ed 2006;45:1557−9.

[71] Cai DY, Song M. Preparation of fully exfoliated graphite oxide nanoplatelets in organic solvents. J Mater Chem 2007;17:3678−80.

[72] Xu C, Wang X, Zhu JW. Graphene-metal particle nanocomposites. J Phys Chem C 2008;112:19841−5.

[73] Petit C, Seredych, Bandosz TJ. Revisiting the chemistry of graphite oxides and its effect on ammonia adsorption. J Mater Chem 2009;19:9176−85.

[74] Hu Y, Kazemian H, Rohani S, Huang YN, Song Y. In situ high pressure study of ZIF-8 by FTIR spectroscopy. Chem Commun 2011;47:12694−6.

[75] Ordoñez MJC, Balkus Jr KJ, Ferraris JP, Musselman IH. Molecular sieving realized with ZIF8/Matrimid® mixed-matrix membranes. J Membr Sci 2010;361:28−37.

[76] Moulder JF, Stickle WF, Sobol PE, Bomben KD, Chastain J, King RC. Handbook of X-ray photoelectron spectroscopy, physical electronics. Eden Prairie, Minn, USA. 1995.

[77] Nie RF, Wang JH, Wang LN, Qin Y, Chen P, Hou ZY. Platinum supported on reduced graphene oxide as a catalyst for hydrogenation of nitroarenes. Carbon 2012;50:586−96.

[78] Storck S, Bretinger H, Maier WF. Characterization of micro- and mesoporous solids by physisorption methods and pore-size analysis. Appl Catal A-Gener 1998;174:137−46.

[79] Dang TT, Zhu YH, Ngiam JSY, Ghosh SC, Chen A, Seayad AM. Palladium nanoparticles supported on ZIF-8 as an efficient heterogeneous catalyst for aminocarbonylation. ACS Catal 2013;3:1406−10.

[80] Wee LH, Janssens N, Sree SP, Wiktor C, Gobechiya E, Fischer RA, et al. Local transformation of ZIF-8 powders and

coatings into ZnO nanorods for photocatalytic application. Nanoscale 2014;6:2056–60.

[81] Wang P, Zhao J, Li XB, Yang Y, Yang QH, Li C. Assembly of ZIF nanostructures around free Pt nanoparticles: efficient size-selective catalysts for hydrogenation of alkenes under mild conditions. Chem Commun 2013;49:3330–2.

[82] Zhou W, Wu H, Hartman MR, Yildirim T. Hydrogen and methane adsorption in metal-organic frameworks: a high-pressure volumetric study. J Phys Chem C 2007;111:16131–7.

[83] Geng Z, Wang DB, Zhang CM, Zhou XY, Xin HF, Liu XP, et al. Spillover enhanced hydrogen uptake of Pt/Pd doped corncob-derived activated carbon with ultra-high surface area at high pressure. Int J Hydrogen Energy 2014;39:13643–9.

[84] Chen CH, Chung TY, Shen CC, Yu MS, Tsao CS, Shi GN, et al. Hydrogen storage performance in palladium-doped graphene/carbon. Int J Hydrogen Energy 2013;38:3681–8.

[85] Wenelska K, Michalkiewicz B, Chen XC, Mijowska E. Pd nanoparticles with tunable diameter deposited on carbon nanotubes with enhanced hydrogen storage. Energy 2014;75:549–54.

[86] Dibandjo P, Zlotea C, Gadiou R, Ghimbeu CM, Cuevas F, Latroche M, et al. Hydrogen storage in hybrid nanostructured carbon/palladium materials: Influence of particle size and surface chemistry. Int J Hydrogen Energy 2013;38:952–65.

[87] Zieliński M, Wojcieszak R, Monteverdi S, Mercy M, Bettahar MM. Hydrogen storage in nickel catalysts supported on active carbon. Int J Hydrogen Energy 2007;32:1024–32.

[88] Kim BJ, Lee YS, Park SJ. A study on the hydrogen storage capacity of Ni-plated porous carbon nanofibers. Int J Hydrogen Energy 2008;33:4112–5.

[89] Zubizarreta L, Menéndez JA, Pis JJ, Arenillas A. Improving hydrogen storage in Ni-doped carbon nanospheres. Int J Hydrogen Energy 2009;34:3070–6.

[90] Suttisawat Y, Rangsunvigit P, Kitiyanan B, Williams M, Ndungu P, Lototskyy MV, et al. Investigation of hydrogen storage capacity of multi-walled carbon nanotubes deposited with Pd or V. Int J Hydrogen Energy 2009;34:6669–75.

[91] Demirocak DE, Ram MK, Srinivasan SS, Kumar A, Goswami DY, Stefanakos EK. Spillover enhancement for hydrogen storage by Pt doped hypercrosslinked polystyrene. Int J Hydrogen Energy 2012;37:12402–10.

[92] Li BY, Huang X, Gong RN, Ma MR, Yang XJ, Liang LY, et al. Catalyzed hydrogen spillover for hydrogen storage on microporous organic polymers. Int J Hydrogen Energy 2012;37:12813–20.

[93] Wang TY, Zhang QJ, Li BH, Chen H, Chen L. Density functional study of hydrogen spillover on direct Pd-doped metal-organic frameworks IRMOF-1. Int J Hydrogen Energy 2012;37:5081–9.

[94] Chien AC, Chuang SSC. Static and dynamic hydrogen adsorption on Pt/AC and MOF-5. Int J Hydrogen Energy 2011;36:6022–30.

[95] Yang SJ, Cho JH, Nahm KS, Park CR. Enhanced hydrogen storage capacity of Pt-loaded CNT@MOF-5 hybrid composites. Int J Hydrogen Energy 2010;35:13062–7.